Astron. Astrophys. 328, 682–688 (1997)

ASTRONOMY AND ASTROPHYSICS

Fine structure in sunspots

I. Sizes and lifetimes of umbral dots

Michal Sobotka[1], **Peter N. Brandt**[2], **and George W. Simon**[3]

[1] Astronomical Institute, Academy of Sciences of the Czech Republic, CZ-25165 Ondřejov, Czech Republic
[2] Kiepenheuer-Institut, D-79104 Freiburg, Germany
[3] PL/GPSS, Sacramento Peak, Sunspot, NM 88349, USA

Received 17 March 1997 / Accepted 19 June 1997

Abstract. The analysis of a 4 1/2 hour series of high resolution white light observations of the umbra in a medium-size sunspot (NOAA 7519, observed on 5 June 1993 at the Swedish Vacuum Solar Telescope, La Palma) is described. An automatic identification and tracking algorithm was applied to umbral dots (UDs) observed in a destretched movie of 360 frames. In total, 662 UDs were tracked and their filling factor, sizes, and lifetimes were measured. It was found that large (diameter $> 0''.4$) and long-lived (lifetime $>$ 10 minutes) UDs appear mostly in regions with enhanced umbral diffuse background intensity. UDs do not have a "typical" size. Their number rapidly increases with decreasing diameter down to the resolution limit. Similarly, UDs do not have a "typical" lifetime, and their number rapidly increases with decreasing lifetime. UDs with lifetimes below 10 minutes represent about 2/3 of the population; the median lifetime is 5.9 minutes.

Key words: Sun: sunspots – physical data and processes: convection – techniques: image processing

1. Introduction

The existence of fine structure in sunspots is well-known: bright and dark filaments in the penumbra, light bridges, umbral dots (UDs), and dark nuclei observed in the umbra. Exceptionally good observational conditions are needed to obtain reliable information about these structures, which are probably related to the interactions of small-scale plasma motions with magnetic fields of different strengths and inclinations. Detailed knowledge of the physical characteristics and the dynamical behaviour of these structures is crucial for our understanding of the origin and evolution of sunspots.

The umbrae and penumbrae of sunspots are dynamical objects; therefore, long time series of high spatial resolution images are required for thorough studies. This is an extremely difficult task because adverse combinations of effects can often thwart such observations: seeing that deteriorates too soon, clouds that appear, instruments that fail, or sunset. Time series of sunspots with appropriate spatial resolution have been obtained only at very few sites around the world: Pic du Midi (e.g. Muller 1973, Kitai 1986), Sacramento Peak (Adjabshirzadeh & Koutchmy 1980), Big Bear (e.g. Ewell 1992, Wang & Zirin 1992), and Canary Islands (e.g. Kusoffsky & Lundstedt 1986). All these authors had to make a rigorous *post facto* selection of frames, and used only a small fraction of the original observing material due to strong variations of image quality. In recent years, the Swedish Vacuum Solar Telescope (SVST, see Scharmer et al. 1985) at La Palma, Canary Islands, has been equipped with an on-line frame-selection system (Scharmer 1989) and a sunspot tracker, which have been continuously improved since their first installation. This has made it possible to acquire several high-quality time series (e.g. Shine et al. 1994, Molowny-Horas 1994, Simon et al. 1994, Sobotka et al. 1995).

UDs are tiny bright features embedded in the dark umbral background. This background itself has a complex structure with smoothly varying intensity, forming brighter and darker regions with diffuse transitions. For this reason we call it *diffuse background*. The darkest regions in the diffuse background, which are almost void of UDs, are termed *dark nuclei* (see Sobotka et al. 1993 for more details concerning the terminology used in this paper). UDs are usually divided into two classes (Grossmann-Doerth et al. 1986): "peripheral" UDs, located in the vicinity of the umbra-penumbra border, and "central" ones in the inner parts of umbra. The "peripheral" UDs are usually brighter than the "central" ones.

Since UDs can be observed only near the resolution limit of contemporary telescopes, their real brightness and size cannot be measured directly. First estimates of the real intensity of UDs, made on the basis of colour temperatures (Beckers & Schröter 1968, Kneer 1973, Koutchmy & Adjabshirzadeh 1981), indicated the brightness of UDs to be close to that of the photosphere. More recent observations revealed intensities in a

Send offprint requests to: M. Sobotka

broader range, often lower than those of the photosphere (Aballe Villero 1992). High spatial resolution spectra made it possible to derive the real brightnesses of UDs from local two-component semi-empirical models and to calibrate a large photometric sample of UDs observed in white-light images (Sobotka et al. 1993). The result showed that, on average, the real brightness of UDs, $I_{\rm ud}$, is proportional to the local brightness of the surrounding diffuse background $I_{\rm db}$, i.e. $I_{\rm ud} \simeq 3 \times I_{\rm db}$. Wiehr (1994) found that the contrast of UDs (with respect to $I_{\rm db}$) decreases with increasing geometrical height. This means that either the intensities of UDs or their sizes, or both, decrease with height.

The real sizes of UDs must be smaller than the observed ones. Their determination is closely related to the estimate of the real brightnesses: if one knows the real and observed brightnesses and the observed size one can calculate the real size from flux conservation. Taking the real brightness equal to the photospheric one, Koutchmy & Adjabshirzadeh (1981) concluded that the diameters of UDs are very small: 0.″14–0.″28 (100–200 km). Aballe Villero (1992), from colour temperature analysis, found the diameters to vary in a broader range: 0.″15–0.″60 (110–440 km). Grossmann-Doerth et al. (1986) and Lites et al. (1991) tried to measure the sizes of UDs in white-light images restored for the estimated instrumental point-spread functions. They obtained 0.″4–0.″9 (290–650 km) and 0.″17–0.″39 (120–280 km), respectively. In the former case, Grossmann-Doerth et al. probably observed clusters of UDs rather than individual ones. Sobotka et al. (1993), using their approximate relation between the $I_{\rm ud}$ and $I_{\rm db}$, derived the diameters to be in the range 0.″25–0.″41 (180–300 km). They also found that the size and brightness of UDs were uncorrelated.

UDs are not static objects. Time series show that they change their brightness and move about. The first estimates of their lifetimes were about 25 minutes (Beckers & Schröter 1968, Adjabshirzadeh & Koutchmy 1980). More recent observations made by Kitai (1986) and Kusoffsky & Lundstedt (1986) indicated longer typical lifetimes of 40 and 60 minutes, respectively. Ewell (1992) reported a mean lifetime of only 15 minutes. Several UDs were observed to exist for more than 2 hours (Kusoffsky & Lundstedt 1986, Ewell 1992). It should be noted that the time resolution of all above mentioned observations was not better than 5 minutes. Those UDs that are located at the periphery of the umbra and sometimes associated with bright penumbral grains, move towards the center of the umbra (Ewell 1992, Molowny-Horas 1994). Ewell suggested distinguishing between "central" and "peripheral" UDs on the basis of their proper motions – "central" UDs were stationary, while "peripheral" UDs drifted inwards. The motion of umbral dots appears to be controlled by the distribution of dark nuclei in the umbra (Sobotka et al. 1995).

In this paper we analyze part of the time series obtained by Simon et al. (1994). This 11 hour series was taken to study horizontal motions in the quiet photosphere, but during 4 1/2 hours a medium-size sunspot was also present in the field-of-view (FOV). The observations and data reduction are summarized in Sect. 2. An automatic identification and tracking algorithm applied to UDs, described in Sect. 3, made it possible to measure intensity variations, effective diameters, lifetimes, and proper motions, of a large number of umbral dots. In Sect. 4 we present the results concerning the filling factor, sizes, and lifetimes of UDs, and summarize and discuss them in Sect. 5. Further results (intensity variations and proper motions of UDs) will be published in a subsequent paper.

2. Observations and data reduction

The observations were performed on 5 June 1993 at the Swedish Vacuum Solar Telescope (SVST), La Palma, Canary Islands. This 50 cm aperture telescope yields a scale of 9.22 arcsec/mm in the primary focus (cf. Scharmer et al. 1985). A magnification system transferred the FOV onto a Kodak Megaplus Model 1.4 CCD camera of 1360 × 1036 pixels with an image scale of 0.125 arcsec/pixel. Typical exposure times were 10 to 14 ms, using a bandpass of 100 Å centered at 4680 Å. The final field size of the recorded images was 1310 × 970 pixels or 164 × 121 arcsec^2. The CCD camera was connected to a DECStation via an 80 Mbyte/s DMA interface and the system was configured such as to work as a "frame selection" device: it sampled frames at a rate of 3.7 Hz, determined the rms granulation contrast in a 256 × 256 pixel sub-area in real time, and stored the two best frames of a 15 s time interval to disk (8 bit digitization). At the end of the interval the data were written onto 8 mm tape which took about 6 s. In this way the two best frames (of a total of 55 samples) from each 21 s interval were recorded. With this setup, an 11 hour series (more than 3700 frames) of unprecedented quality and duration was observed. For the whole series the granulation contrast, determined in a field far away from any activity, was mostly between 6% and 10.6% rms without any corrections applied. The best images of this series show details of granular structures near the diffraction limit of the telescope. Some first results on large-scale photospheric motions derived from this series were published by Simon et al. (1994).

The FOV contained the sunspot group NOAA 7519 (Fig. 1) at position N05, E15. The group was in the maximum phase of evolution on the date of observation. The leading and largest spot consisted of four umbral cores separated by three strong light bridges. The telescope drifts and low-frequency components of image motion due to seeing were minimized using a quad-cell sunspot tracker whose working principle was described by von der Lühe (1988). During the observing sequences, the tracker was locked on a small sunspot in the middle of the group, seen in the lower right corner of Fig. 1. Due to the altazimuth construction of the telescope, the observed FOV rotated around this locking point. Since the main aim of the observing run was the study of horizontal motions in the quiet photosphere, the large spot of the group was in the FOV only part of the time. Therefore we selected a subset from 9:54 to 14:20 UT consisting of 760 frames (one per 21 s selection interval) showing the whole sunspot.

After dark current and flat field corrections, we de-rotated the frames around the pivot point. The average photospheric intensity in all frames was normalized to unity to compensate for changes of transparency and/or exposure time. The frames were

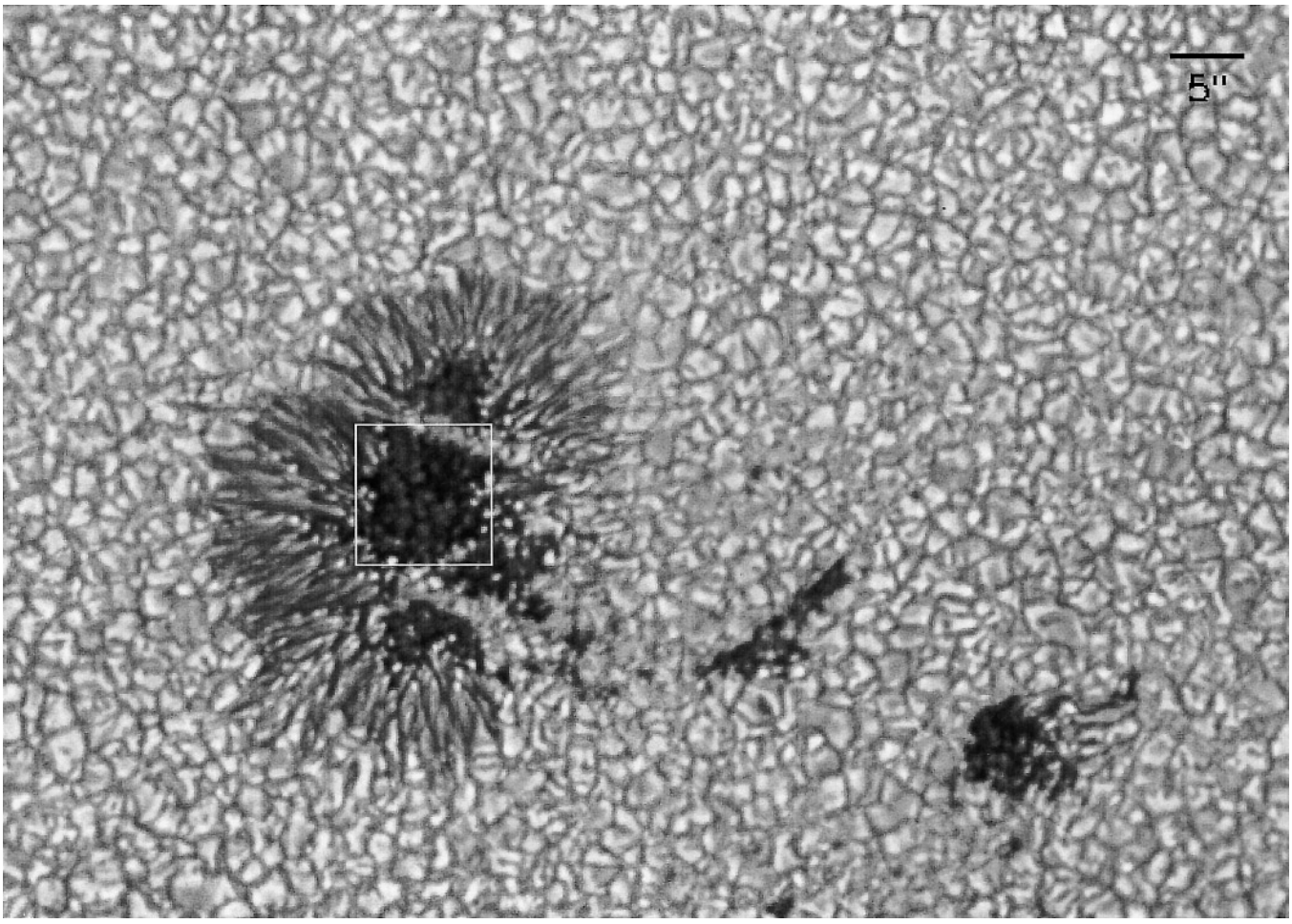

Fig. 1. Image of sunspot group NOAA 7519, observed at 12:08:44 UT on 5 June 1993, showing the analyzed umbral core (box size $8\farcs75 \times 8\farcs75$) of the leading spot (left) and the small spot (right) used for tracking. The image was numerically sharpened for better presentation. This figure shows approximately 1/4 of the whole field-of-view.

then registered to remove residual large-scale image motions (rigid alignment). The correction for theoretical instrumental profile of the telescope and the noise filtering were carried out simultaneously by means of a Wiener filter (as described by Sobotka et al. 1993). In order to minimize seeing distortions, the images were destretched using modifications of routines written by Molowny-Horas & Yi (1993). The destretching was applied in three consecutive steps, removing successively large- and small-scale deformations, and residual jitter. The reference frames for destretching were determined individually for each image as averages of time subseries of 5 or 7 frames surrounding the image to be destretched. This enabled us to eliminate the seeing-induced shifts and preserve the real motions. Since we wished to keep the information about waves and oscillations in the umbra, we did not apply any $k-\omega$ filtering. We find that intensity oscillations in the umbra are negligible and thus have no effect on measurements of UD lifetimes.

In order to retain only the frames of highest quality, for the final analysis we selected frames of contrast $> 6.6\%$ rms and time lags > 29 s, yielding 360 frames covering almost regularly the whole time period. This choice of selection parameters represented a compromise between quality and time coverage. It should be noted that the rms contrast for this selection was determined in an area near the spot, so that the values, possibly influenced by abnormal granulation, are slightly lower than the original ones. Comparing both sets of rms values we can state that the final series contains images corresponding to quiet granulation rms contrasts $\gtrsim 7.6\%$.

Due to differential seeing, the image quality changes from one location in the FOV to another. To determine the reliability of the photometric measurements, we needed an image quality criterion applicable to the location where the measurement was made, i.e. the sunspot itself. Since an rms contrast measurement in the umbra would not make much sense, we used an auxiliary measure of the image quality – the "image sharpness". This was defined as the mean value of the image after applying the Roberts gradient operator (a 2×2 diagonal matrix with elements -1 and 1). In our case, the image sharpness was measured in a 100×100 pixel ($12\farcs5 \times 12\farcs5$) area containing the central umbral core, two light bridges, and the inner parts of the penumbra. To check the consistency of image sharpness with the rms granulation contrast we compared the curves of temporal variations of both

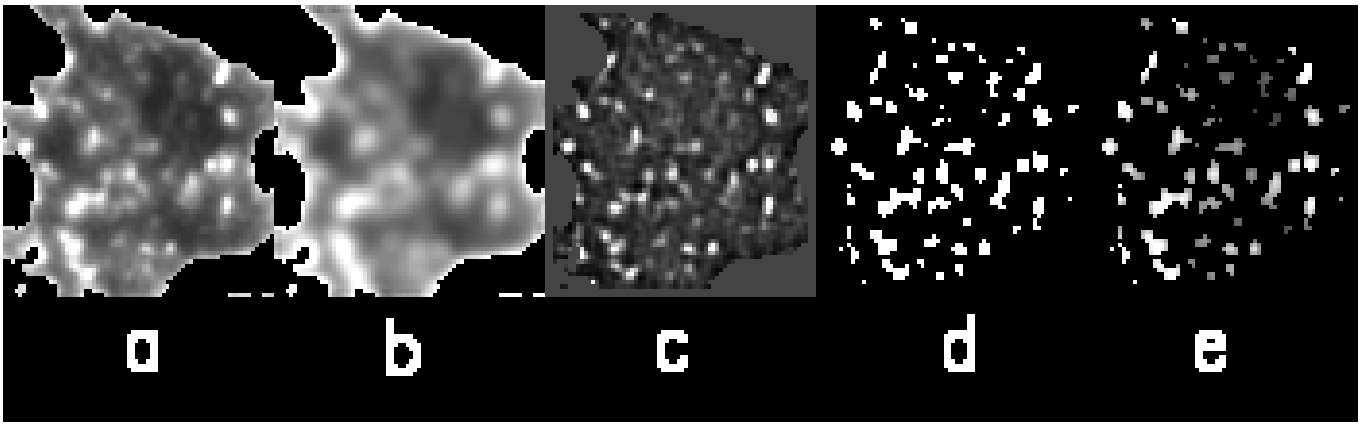

Fig. 2a–e. Demonstration of image segmentation for one frame of the series. **a** Original image of the umbral core; **b** original smoothed by a boxcar $0\farcs625 \times 0\farcs625$; **c** differential image [**a**−**b**]; **d** binary mask; **e** segmented image [**a** × **d**]. The field is $8\farcs75 \times 8\farcs75$.

quantities during the whole series and found that they have a very similar shape and display the periods of excellent, as well as of lower, image quality in a consistent manner.

For the purpose of a time series analysis, the selected frames were interpolated in time to obtain a constant time lag of 44.5 s between successive frames. The image sharpness after this interpolation was reduced on average by a factor of 0.97.

Since our data were not designated originally for the study of sunspots, no specific stray light determination was made during the observation. We believe that the core of the seeing point-spread function (PSF) is very narrow thanks to short exposure time and image selection – this is confirmed by the high values of the rms granulation contrast. However, we have no information about the far wings of the PSF which represent scattered light. Although the amount of scattered light at the SVST is usually below 1% at 4680 Å, we must consider the observed intensities and sizes of UDs as apparent and relative values. This is not a drawback in the case of time series, where temporal changes are of prime concern.

3. Image segmentation, identification, and tracking of objects

For further analysis we selected an $8\farcs75 \times 8\farcs75$ (70 × 70 pixel) field covering the large central umbral core of the leading sunspot (see box in Fig. 1). This umbral core contained 5 dark nuclei and a varying number of UDs. The boundary of the umbral core was defined individually in each frame at the iso-intensity level of 0.45 $I_{\rm phot}$ after $0\farcs875 \times 0\farcs875$ boxcar smoothing (which was done to eliminate the ragged borders of the umbral core). The intensity signal in the region outside the umbral core was set to zero.

UDs were isolated individually in each frame of the umbral core using a simple image segmentation method, based on an edge enhancement algorithm: For each frame a differential image was computed by subtracting a smoothed image (boxcar $0\farcs625 \times 0\farcs625$) from the original one. From this differential image we computed a binary mask, setting pixel values higher than an empirically estimated threshold (0.015) to 1 and the rest to 0. The original image was then multiplied by this mask, producing a segmented image in which the bright peaks (UDs) conserved their original intensity, and the background was set to zero. An example of this image segmentation process is shown in Fig. 2.

To identify and track UDs in time, we developed a procedure with the following criteria: The objects under study (UDs) are formed from the non-zero intensity pixels. Only side-by-side neighbouring pixels belong to the same object. Single-pixel objects are considered noise and rejected. Pixels forming an object are labelled by an object identification number which, together with the pixel coordinates, is stored in memory. In the next step, the spatial coincidences of objects in each pair of subsequent frames are investigated. Two objects are identified as predecessor/successor if they coincide in the coordinates of at least one pixel in both frames. Formation, death, splitting, and merging of objects are taken into account. In the case of splitting, the brightest object is adopted as the successor, while if merging occurs, the predecessor of the merged object is identified as the object with the longest history. In moments of poor seeing some objects may "disappear" (they are not resolved) in one or more frames and then reappear when the seeing gets better. If the object is missing in only 1 or 2 successive frames, and the distance between the locations of disappearance and reappearance is less than $0\farcs3$, the history of the object (record of the maximum intensity together with its coordinates and the total number of pixels in the object) is regarded as uninterrupted.

To improve the reliability of the results we exclude all objects with lifetimes shorter than 3 frames (89 s). Variable image quality may cause spurious merging and splitting which can make independent objects appear related. This would lead to large displacements of the maximum intensity positions and to unrealistic velocities of proper motions. This problem can be partially fixed by elimination of objects with velocities larger than 1 km/s, since we do not expect such velocities in the umbra (cf. Kitai 1986, Molowny-Horas 1994, Sobotka et al. 1995).

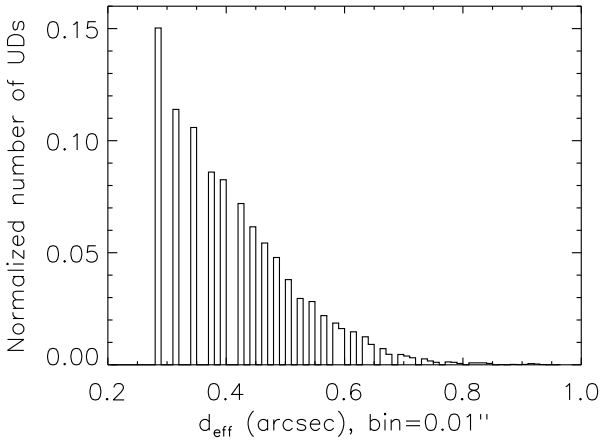

Fig. 3. Normalized number of UDs vs. observed effective diameter $d_{\rm eff}$ for 11758 instantaneous measurements.

After applying these restrictions, we obtained a sample of 662 UDs which we used for further statistical analysis. From the procedure described above, we obtained the lifetimes of the objects (given by the number of frames in which the objects are present) and for each frame the magnitude and position of the maximum intensities and the effective diameters, derived from the number of pixels (area), of the objects. The average proper motion velocities of the features were calculated from their positions by means of least-squares linear fits (cf. Molowny-Horas 1994). The results concerning the intensity variations and proper motions will be described in a separate paper.

4. Results

First we summarize some global characteristics of the umbral core under investigation: its size, the number of UDs, and filling factor of UDs (ratio of the total area of UDs to the area of the umbral core). The area A (in pixels) of the umbral core was defined using the iso-intensity level of 0.45 $I_{\rm phot}$, as described in Sect. 3. From this we calculated the effective diameter $d_{\rm eff} = 0\farcs125\sqrt{4A/\pi}$. It decreased during the 4 hour 26 minute period from $8\farcs6$ to $8\farcs0$. In the linear approximation (least-squares fit) the umbral core area decreased at a rate of -3.1 % per hour.

To obtain the number and filling factor of UDs in the umbral core we excluded all bright objects formed by only 2 or 3 pixels, i.e. with $d_{\rm eff}$ smaller than the resolution limit of the telescope ($0\farcs25$). The average number of UDs in the umbral core was 33 ± 5. It varied between 16 and 47 UDs in correlation with the image sharpness (correlation coefficient $C = 0.6$), but did not show any regular trend in time. The observed filling factor (based on the "observed sizes" of UDs) was $8.9\% \pm 1.5\%$; its temporal variations were also correlated with the image sharpness ($C = 0.8$), with no regular time-trend. We conclude that during the 4 1/2 hour period the number of UDs and the filling factor remain practically constant and their temporal variations are due mostly to changes in image quality.

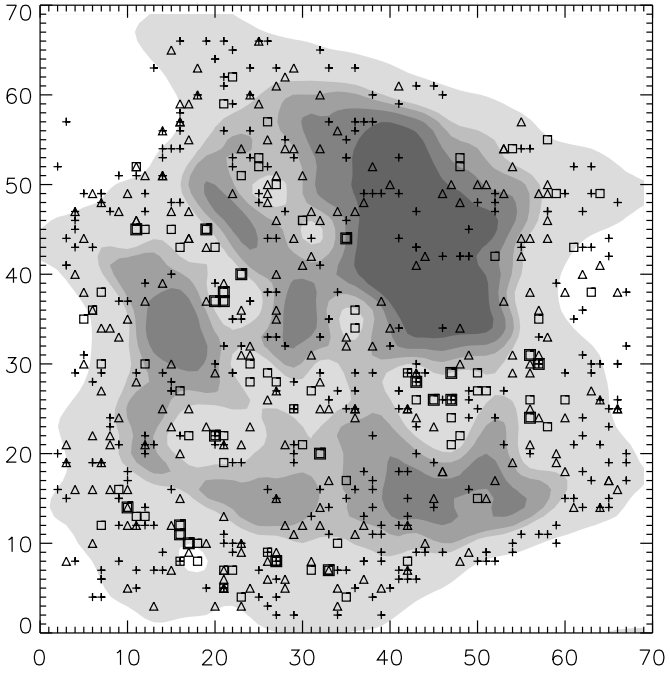

Fig. 4. Spatial distribution of 662 UDs with different time-averaged effective diameters $\overline{d_{\rm eff}}$: Symbol "+" represents UDs with $\overline{d_{\rm eff}} \leq 0\farcs3$, triangles correspond to $0\farcs3 < \overline{d_{\rm eff}} \leq 0\farcs4$, squares to $0\farcs4 < \overline{d_{\rm eff}} \leq 0\farcs5$, and bold squares to $\overline{d_{\rm eff}} > 0\farcs5$. The underlying grey-scale image of the umbral core is the average of 360 frames of the series with contours corresponding to intensities 0.24, 0.26, 0.28, 0.30, and 0.45 $I_{\rm phot}$. The coordinates are in pixels (scale $0\farcs125$ per pixel).

4.1. Effective diameters of umbral dots

We remind the reader that the effective diameters $d_{\rm eff}$ of UDs presented here correspond to the "observed sizes", which are influenced by image blurring (see Sect. 1). To obtain a histogram of $d_{\rm eff}$ (Fig. 3) we utilized 11758 observations of *instantaneous* sizes of UDs disregarding their temporal evolution. This has the disadvantage of collecting statistically dependent elements due to the short time spacing between images, but it has the strong advantage of providing a large sample to achieve high statistical significance.

The average value of $d_{\rm eff}$ is $0\farcs42 \pm 0\farcs12$, in good agreement with the mean observed diameter reported by Sobotka et al. (1993) ($0\farcs43 \pm 0\farcs10$). The histogram in Fig. 3 is asymmetric, with the number of UDs strongly increasing toward the resolution limit. The tail of the histogram for $d_{\rm eff} \gtrsim 0\farcs6$ is probably due to unresolved clusters of UDs rather than to individual ones. This size distribution of UDs is not sensitive to image quality or the level of segmentation: Increasing the image quality selection criterion from 6.6% to 8.5% reduced the number of frames from 360 to 52, but showed nearly no change in the shape of the histogram; increasing the segmentation level from 0.015 to 0.02 in the differential image induced only slight changes in the histogram. *We conclude that UDs do not have a "typical" diameter; rather, the smaller the UDs, the more numerous they are.*

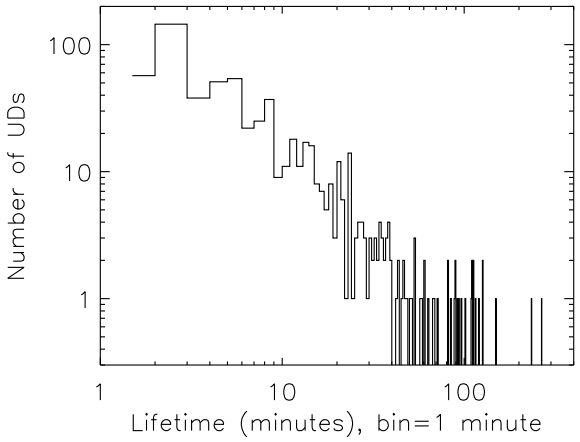

Fig. 5. Number of UDs vs. lifetime for 662 UDs.

To show the spatial distribution of UDs of different $d_{\rm eff}$ (Fig. 4) we calculated the time-averaged effective diameters $\overline{d_{\rm eff}}$ of the 662 UDs. We see that large UDs ($\overline{d_{\rm eff}} > 0\farcs4$) preferentially appear in the bright parts of the umbral core, while small UDs are distributed more or less randomly. The histogram of $\overline{d_{\rm eff}}$ has a shape similar to that of $d_{\rm eff}$ (Fig. 3). From this we conclude that Fig. 3 shows a real distribution of observed sizes of UDs – and is not distorted by transient phenomena like speckles.

4.2. Lifetimes of umbral dots

The histogram of the lifetimes is shown in Fig. 5. The minimum lifetime, 89 s, was set by the tracking algorithm, which, for the sake of reliability, excluded all objects which appeared only in one or two frames. The number of UDs rapidly decreases with increasing lifetime. We find that 66% of UDs have lifetimes shorter than 10 minutes, 27% between 10 and 40 minutes, 6% between 40 and 120 minutes, while only 1% of UDs exist longer than 2 hours. We cannot see any peaks in the histogram. *We conclude, therefore, that the 662 UDs in this sample do not have a "typical" lifetime*. The average lifetime is 13.8 minutes, and the median 5.9 minutes.

We display in Fig. 6 the spatial distribution of UDs with different lifetimes. We see that long-lived UDs (lifetime $>$ 40 minutes) appear in bright parts of the umbral core at locations similar to those of UDs with large $\overline{d_{\rm eff}}$. We show the relation between lifetimes and time-averaged sizes of UDs with a scatter diagram (Fig. 7). It indicates that the minimum size of UDs increases with lifetime.

5. Discussion and conclusions

In a 4 1/2 hour time series of excellent quality a sample of 662 UDs, obtained by an object-tracking procedure, was analyzed with the following results:

1. The observed filling factor of UDs in the umbral core was 8.9% $\pm$ 1.5% on average. This is consistent with the earlier estimate made by Sobotka et al. (1993). During the 4 1/2 hour period the number of UDs and the filling factor remained practically constant.

2. Large (diameter $> 0\farcs4$) and long-lived (lifetime $>$ 10 minutes) UDs appear mostly in regions with enhanced umbral diffuse background intensity. In such regions the magnetic field strength is expected to be smaller than in dark areas (Kopp & Rabin 1992, Martínez Pillet & Vázquez 1993, Solanki et al. 1993).

3. UDs do not have a "typical" size. Their number rapidly increases with decreasing diameter down to the resolution limit.

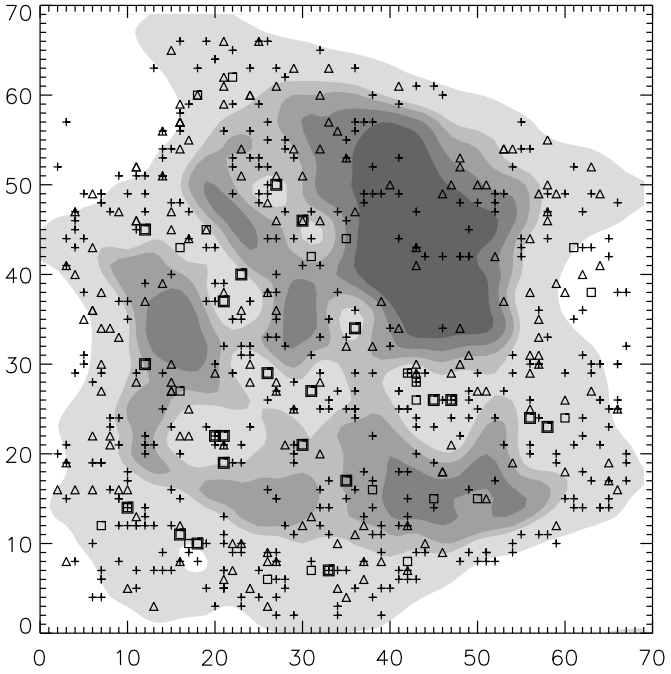

Fig. 6. Spatial distribution of UDs with different lifetimes t: Symbol "+" represents UDs with $t \leq 10$ minutes, triangles correspond to $10 < t \leq 40$ minutes, squares to $40 < t \leq 80$ minutes, and bold squares to $t > 80$ minutes. The underlying image and scale are as in Fig. 4.

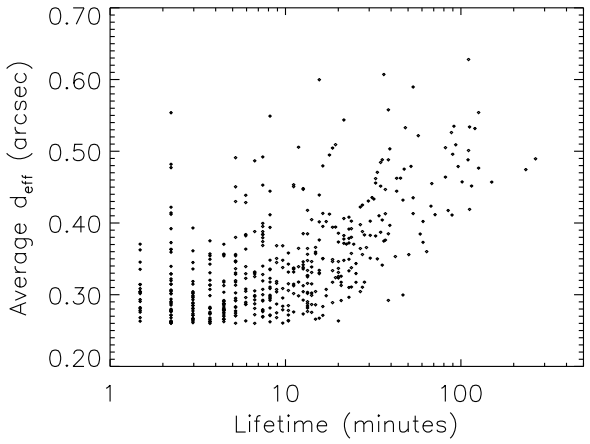

Fig. 7. Scatter diagram of effective diameter $\overline{d_{\rm eff}}$ vs. lifetime.

This is a somewhat surprising result, in contradiction to several previous estimates of UD sizes (Koutchmy & Adjabshirzadeh 1981, Grossmann-Doerth et al. 1986, and Sobotka et al. 1993). The deficit of small UDs in those observations is probably due to the visual nature of the object search, so that selection effects led to discarding of smaller and less contrasty objects. (It can be demonstrated with our present sample of UDs that their observed contrast with respect to the local diffuse background decreases for $d_{\rm eff} < 0\farcs35$ due to the image degradation caused by blurring and telescope resolution.) Our result stems from a larger and better-quality data set and a new object-tracking algorithm, which we believe is more objective than previous methods. It is very interesting to compare the histogram of $d_{\rm eff}$ of UDs (Fig. 3) with that of photospheric granules (see e.g. Fig. 6 in Roudier & Muller 1986). These distributions have nearly identical shapes.

4. UDs do not have a "typical" lifetime. Short-lived UDs (lifetimes below 10 minutes) represent about 2/3 of the population, while only 1% live more than 2 hours. This is again a new and unexpected result, obtained by the object-tracking algorithm. It differs from the estimates of characteristic lifetimes of 15 to 60 minutes reported by Adjabshirzadeh & Koutchmy (1980), Kitai (1985), Kusoffsky & Lundstedt (1986), and Ewell (1992). Their data were based on small samples of UDs, probably influenced by visual selection effects, and had a low temporal resolution (5 minutes in the best case). Moreover, their measurements of lifetimes may also have been affected by temporal intensity variations of long-lived UDs. However, Kitai (1985) also reported a similar distribution of lifetimes for a sample of 55 "chromospheric umbral dots", bright features with sizes about $1''$, observed in Hα filtergrams.

Acknowledgements. We acknowledge the efficient support by M. Barreto, G. Hosinsky, R. Kever, G. Scharmer, and W. Wang during the observations at La Palma. The sunspot tracker was developed and built by the ETH Zürich astronomy group under the leadership of C. Keller. Technical and financial support was provided by Mark Shand of DEC's Paris office. M. S. gratefully acknowledges grants by the Deutsche Forschungsgemeinschaft (436 TSE 17/5/95) and by the Grant Agency of the Academy of Sciences of the Czech Republic (A 3003601). This work was accomplished under the Key Project K1-003-601 of the Academy of Sciences of the Czech Republic. The Swedish Vacuum Tower Telescope is operated by the Swedish Royal Academy of Sciences at the Spanish Observatorio del Roque de los Muchachos of the Instituto de Astrofísica de Canarias. Both the Air Force Office of Scientific Research and the Kiepenheuer-Institut für Sonnenphysik provided support to G.W.S. for this project, while P.N.B. received travel funds from AFOSR's European Office of Aerospace Research.

References

Aballe Villero M. A., 1992, Thesis, Univ. La Laguna
Adjabshirzadeh A., Koutchmy S., 1980, A&A 89, 88
Beckers J. M., Schröter E. H., 1968, Solar Phys. 4, 303
Ewell M. W., 1992, Solar Phys. 137, 215
Grossmann-Doerth U., Schmidt W., Schröter E. H., 1986, A&A 156, 347
Kitai R., 1986, Solar Phys. 104, 287
Kneer F., 1973, Solar Phys. 28, 361
Kopp G., Rabin D., 1992, Solar Phys. 141, 253
Koutchmy S., Adjabshirzadeh A., 1981, A&A 99, 111
Kusoffsky U., Lundstedt H., 1986, A&A 160, 51
Lites B. W., Bida T. A., Johannesson A., Scharmer G. B., 1991, ApJ 373, 683
von der Lühe O., 1988, A&A 205, 354
Martínez Pillet V., Vázquez M., 1993, A&A 270, 494
Molowny-Horas R., 1994, Solar Phys. 154, 29
Molowny-Horas R., Yi Z., 1993, in: Proc. of the 8th Scandinavian Conference on Image Analysis, eds. K. A. Høgda, B. Braathen, K. Heia
Muller R., 1973, Solar Phys. 29, 55
Roudier T., Muller R., 1986, Solar Phys. 107, 11
Scharmer G.B., Brown D.S., Pettersson L., Rehn J., 1985, Appl. Optics 24, 2558
Scharmer G.B., 1989, in: Solar and Stellar Granulation, eds. R. J. Rutten, G. Severino, Kluwer, Dordrecht, p. 161
Shine R. A., Title A. M., Tarbell T. D., Smith K., Frank Z. A., 1994, ApJ 430, 413
Simon G. W., Brandt P. N., November L. J., Scharmer G. B., Shine R. A., 1994, in: Solar Surface Magnetism, eds. R. J. Rutten, C. J. Schrijver, Kluwer, Dordrecht, p. 261
Sobotka M., Bonet J. A., Vázquez M., 1993, ApJ 415, 832
Sobotka M., Bonet J. A., Vázquez M., Hanslmeier A., 1995, ApJ 447, L133
Solanki, S. K., Walther, U., Livingston, W., 1993, A&A 277, 639
Wang H., Zirin H., 1992, Solar Phys. 140, 41
Wiehr E., 1994, A&A 287, L1

This article was processed by the author using Springer-Verlag LaTeX A&A style file *L-AA* version 3.